TTP99-12*
DESY 99-031
hep-ph/9903322
March 1999

Axial Contributions at the Top Threshold

J.H. Kühn

Institut für Theoretische Teilchenphysik, Universität Karlsruhe, D-76128 Karlsruhe, Germany

T. Teubner

Deutsches Elektronen-Synchrotron DESY, D-22603 Hamburg, Germany

Abstract

We calculate the contributions of the axial current to top quark pair production in e^+e^- annihilation at threshold. The QCD dynamics is taken into account by solving the Lippmann-Schwinger equation for the P wave production using the QCD potential up to two loops. We demonstrate that the dependence of the total and differential cross section on the polarization of the e^+ and e^- beams allows for an independent extraction of the axial current induced cross section.

Top quark production at an electron-positron collider [1] has been demonstrated to be ideally suited for a precise determination of the top quark mass and for the study of its couplings in production and decay. Due to its rapid decay large distance nonperturbative QCD effects are irrelevant for the description of the top quark [2], and the $t\bar{t}$ system is well described by perturbative QCD [3]. It allows to explore the interquark potential at small distances, which is closely related to the strong coupling constant. One might eventually even become sensitive to the t-$\bar{t}$-Higgs coupling through virtual corrections. In order to constrain this multitude of parameters in an optimal

*The complete postscript file of this preprint, including figures, is available via anonymous ftp at www-ttp.physik.uni-karlsruhe.de (129.13.102.139) as /ttp99-12/ttp99-12.ps or via www at http://www-ttp.physik.uni-karlsruhe.de/cgi-bin/preprints.

way and to reduce inevitable theoretical uncertainties, it is desirable to measure a large variety of different observables. Originally the main emphasis had been put on the total cross section [3, 4]. The excitation curve with its steep rise (the remnant of the $1S$ toponium resonance) is ideally suited for the measurement of the top quark mass m_t. The correlation between m_t and the strength of the potential (α_s) can be reduced by comparing data and predictions for the momentum distribution of the top quarks [5, 6, 7, 8], which reflects essentially their Fermi motion in the bound state and the smearing of the momentum due to the large decay rate Γ_t, a consequence of the uncertainty principle. All these quantities were calculated for the S wave amplitude, which is induced by both the electromagnetic current and the vector part of the neutral current close to threshold. Expanding in the limit of small velocities $\beta = \sqrt{1-4m_t^2/s}$ ($\sqrt{s}$ being the total centre of mass energy), the next term is due to $S-P$ wave interference. The subleading P wave amplitude originates from the production through the axial vector current. The interference term is responsible for the anisotropic angular dependence, specifically the term linear in $\cos\theta$, and the resulting forward-backward asymmetry [9]. Similarly, an angular dependent polarization of top quarks is induced by the $S-P$ wave interference which adds to the dominant polarization parallel to the e^+e^- beams [10]. Rescattering corrections [11, 12], although important for the detailed quantitative analysis, do not alter this qualitative picture.

Clearly, the next step in this sequence of improvements are corrections of order β^2 which, for interacting quarks close to threshold, translate into corrections of order α_s^2 and $\beta\alpha_s$. For the vector current this has been recently persued by different groups, which have demonstrated the importance of these next-to-next-to leading order corrections [13, 14, 15]. However, in the same order β^2 (or α_s^2) also axial vector induced contributions must be incorporated. They affect both the excitation curve and the momentum distribution. Close to threshold these axial contributions are suppressed relative to the dominant S waves by two powers of β whence a treatment of the leading terms is sufficient for the present purpose. These axial contributions are mediated by the virtual Z boson only. Therefore their dependence on the beam polarization differs from the one of the vector current induced rate. This, in turn, allows for the separation of the two independent contributions to the total and differential cross section. With the axial contribution representing an independent observable, this separation is possible independent of potential uncertainties in the NNLO calculation of the dominant piece. However, in view of the β^2 suppression of the axial rate and the relatively small couplings of the neutral current, large luminosities and a high degree of polarization are required to make a clean extraction of the axial part possible. These features are unique for linear colliders, as proposed e.g. in [1, 16]. However, even without this possibility, it will be important to control the impact of this contribution on the extraction of the top quark mass and the interquark potential. Let us also stress that the axial

rate, although closely related to the $S-P$ wave interference piece, is an independent observable. Rescattering corrections, which are present in the angular distribution and in the top polarization, are calculated to $\mathcal{O}(\alpha_s)$ [11, 12] but shown to be unimportant as long as the total cross section is concerned [17, 18]. In addition, rescattering corrections do not affect the separation between axial and vector contributions.

P wave threshold production of massive quarks in $\gamma\gamma$ collisions has been analysed for the case of a pure Coulomb potential in Ref. [19] and much of the general considerations can be taken over to the present case.[1] This refers in particular to the treatment of the linearly divergent integrals over the momentum distribution and the order of magnitude estimates. However, for definite predictions the QCD potential with its logarithmically varying coupling strength has to be employed. The relative size of the electromagnetic and weak couplings is important for the phenomenological analysis, as well as the dependence on the beam polarization.

The momentum distribution of the top quark including the influence of beam polarization can be written in the form

$$\begin{aligned}\frac{\mathrm{d}\sigma}{\mathrm{d}p} &= \frac{3\alpha^2\Gamma_t}{m_t^4}\,(1-P_+P_-)\left[(a_1+\chi a_2)\left(1-\frac{16}{3}\frac{\alpha_s}{\pi}\right)\mathcal{D}_{S-S}(p,E)\right.\\ &\qquad\left.+\,(a_5+\chi a_6)\left(1-\frac{8}{3}\frac{\alpha_s}{\pi}\right)\mathcal{D}_{P-P}(p,E)\right]\,, \qquad (1)\end{aligned}$$

where the correction factors from hard gluon exchange, $(1-16\alpha_s/3\pi)$ and $(1-8\alpha_s/3\pi)$, are taken from [22, 23]. P_+ and P_- denote the polarization of the positron and electron beams, respectively, and χ is defined as

$$\chi = \frac{P_+ - P_-}{1-P_+P_-}\,. \qquad (2)$$

The coefficients a_i read

$$\begin{aligned} a_1 &= (q_e q_t + v_e v_t d)^2 + (a_e v_t d)^2\,, & a_2 &= 2a_e v_t d\,(q_e q_t + v_e v_t d)\,,\\ a_5 &= (a_t d)^2\left(v_e^2+a_e^2\right)\,, & a_6 &= 2v_e a_e\,(a_t d)^2\,, \end{aligned} \qquad (3)$$

with

$$d = \frac{1}{16\sin^2\theta_W\cos^2\theta_W}\,\frac{s}{s-M_Z^2} \qquad (4)$$

and the electromagnetic and weak charges

$$\begin{aligned} q_e &= -1\,, & v_e &= -1+4\sin^2\theta_W\,, & a_e &= -1\,,\\ q_t &= 2/3\,, & v_t &= 1-8/3\,\sin^2\theta_W\,, & a_t &= 1\,. \end{aligned} \qquad (5)$$

[1] See also Refs. [20] and [21] for related discussions of P wave production of quarks and squarks in e^+e^- collisions near threshold.

The dynamics of the strong interaction is contained in the functions

$$\mathcal{D}_{S-S}(p,E) = p^2\,|G(p,E)|^2 \qquad \text{and} \qquad \mathcal{D}_{P-P}(p,E) = p^2\left|\frac{p}{m_t}\,F(p,E)\right|^2 , \tag{6}$$

where $E = \sqrt{s} - 2m_t$ is the energy relative to the nominal threshold. The S and P wave Green functions $G(p,E)$ and $F(p,E)$ fulfill the Lippmann-Schwinger equations

$$G(p,E) = G_0(p,E) + G_0(p,E)\int \frac{\mathrm{d}^3q}{(2\pi)^3}\,\tilde{V}\,(\,|\,\vec{p}-\vec{q}\,|\,)\,G(q,E)\,, \tag{7}$$

$$F(p,E) = G_0(p,E) + G_0(p,E)\int \frac{\mathrm{d}^3q}{(2\pi)^3}\frac{\vec{p}\cdot\vec{q}}{p^2}\,\tilde{V}\,(\,|\,\vec{p}-\vec{q}\,|\,)\,F(q,E) \tag{8}$$

where $p = |\,\vec{p}\,|$ is the momentum of the top quark in $t\bar{t}$ rest frame, $G_0(p,E) = (\,E - p^2/m_t + \mathrm{i}\Gamma_t\,)^{-1}$ is the free Green function, and Γ_t denotes the top quark width. For the QCD potential in momentum space, $\tilde{V}$, we adopt the two loop result [24] with the long distance regularization as described in [25]. Eqs. (7, 8) are then solved numerically as described in [6, 26]. For all the results discussed below we use the parameters $m_t = 175$ GeV, $\Gamma_t = 1.43$ GeV and $\alpha_s(M_Z^2) = 0.118$.

For large momenta both $G(p,E)$ and $F(p,E)$ approach the free Green function G_0. It is thus evident that the integral over the momentum distribution diverges linearly for the P wave. This is, however, an artefact of the nonrelativistic approximation. The problem could be cured, for example, by introducing in this region the relativistic (free) Green function and phase space and by treating the interaction as a (small) perturbation. However, in practice, a cutoff will be provided by the experimental analysis. The invariant mass of the W plus b jet in events with large p (Wb) and small $E = \sqrt{s} - 2m_t$ will necessarily be strongly shifted away from m_t towards smaller values. Such events will either not be included in the $t\bar{t}$ sample or, in any case, will require special treatment. Hence, wherever total cross sections are presented, a cutoff $p_{\max}$ of order m_t will be introduced which is easily included also in the experimental analysis.

The relative magnitude of the P wave result is best visualized by considering the basic elements $\mathcal{D}_{S-S}$ and $\mathcal{D}_{P-P}$ which enter Eq. (1). In Fig. 1 we show these distributions for three energies, $E = -3$, 0 and 3 GeV. These energies roughly correspond to the location of the $1S$ peak, the nominal threshold and the onset of the continuum. For the S wave (Fig. 1a) we observe a fairly wide distribution at $E = -3$ GeV, a consequence of the momentum spread of the constituents in the $1S$ bound state. With increasing energy the interaction becomes less important, the width of the distribution decreases and approaches the free result $\Gamma_t\sqrt{m_t/E}$. For the P wave (Fig. 1b) the contribution is tiny at $E = -3$ GeV and develops a peak only gradually with increasing energy. The ratio $\mathcal{D}_{S-S}/\mathcal{D}_{P-P}$ is shown in Fig. 1c. For energies well above threshold its behaviour is essentially given by the factor p^2/m_t^2, since both F and G are approximated by the

free Green function G_0. However, for energies relatively close to threshold the strong interaction distorts the free wave functions which leads to a deviation from the pure p^2/m_t^2 behaviour. The ratio of the integrated S and P wave distributions as functions of E is shown in Fig. 2a. The different curves give the results for different values of the momentum cutoff $p_{\rm max}$ which is applied both in numerator and denominator. For a realistic analysis $p_{\rm max} = m_t/3$ or $m_t/2$ should be used at most. For free and stable quarks the ratio is given by $p^2(E)/m_t^2 \approx E/m_t$. Fig. 2a shows that close to threshold the momentum spread from the QCD bound state dynamics leads to a significant modification of the E/m_t behaviour and increases the P wave contribution. The minimum of the ratio $\int_0^{p_{\rm max}} {\rm d}p\, \mathcal{D}_{P-P} \,/\, \int_0^{p_{\rm max}} {\rm d}p\, \mathcal{D}_{S-S}$ is observed roughly at the location of the remnant of the $1S$ peak of the $R_{t\bar{t}}$ ratio (Fig. 2b)

$$R_{t\bar{t}} \equiv \frac{\sigma(e^+e^- \to \gamma^* \to t\bar{t}\,)}{\sigma(e^+e^- \to \gamma^* \to \mu^+\mu^-)} = \frac{4\Gamma_t}{\pi m_t^2} \int_0^{p_{\rm max}} {\rm d}p\, \mathcal{D}_{S-S}\,. \tag{9}$$

With these ingredients it is now straightforward to predict the differential distribution for the three characteristic polarizations $P_- = -1,\ 0,\ +1$ and $P_+ = 0$. The cross sections are drastically different for the three choices, see Fig. 3, reflecting the large left–right asymmetry $A_{\rm LR} = a_2/a_1 \approx 0.4$ of the S wave contribution [2, 27]. Including the small P wave term (dotted curves) leads to marginal changes only, which are barely visible in Fig. 3 even for the highest energies. The relative size of the axial contribution is better visible in Fig. 4 where the ratio between the axial and the vector contribution is plotted as a function of the momentum p. The shapes and the magnitude are fairly similar for the different energies. This is a consequence of the fact, that the ratio $\mathcal{D}_{P-P}(p,E)/\mathcal{D}_{S-S}(p,E)$ is relatively insensitive to the energy. In fact, in the absence of interaction this ratio is just given by p^2/m_t^2, independent of E. In contrast, the location of the maximun of the distribution itself varies with E, and this is mainly responsible for the increase of the integrated P wave cross section. The integrated cross section with and without the P wave contribution is shown in Fig. 5a, where for the cutoff $p_{\rm max} = m_t/2$ is adopted. The ratio between axial and vector contributions, both integrated up to $m_t/2$ is shown in Fig. 5b. The shape of these curves reflects the shape of the ratio $\int {\rm d}p\, \mathcal{D}_{P-P} \,/\, \int {\rm d}p\, \mathcal{D}_{S-S}$ displayed already in Fig. 2a. The normalization depends on the polarization. This demonstrates that experiments with polarized beams are able to extract $\sigma_{\rm tot}^{\rm AA}$ separately, provided that a statistical and systematic precision at the percent level can be reached. In any case, if a theoretical prediction of shape and normalization of ${\rm d}\sigma/{\rm d}p$ at a precision of one or two percent is needed the P wave contribution to the cross section should be included.

Acknowledgments

We thank Robert Harlander for providing us with the implementation of polarization and P wave contributions in TOPPIK and for useful discussions. Work partly supported by BMBF Contract 056 KA 93 P6 at the University of Karlsruhe.

References

[1] E. Accomando et al., *Phys. Rep.* **299** (1998) 1.

[2] J.H. Kühn, *Acta Phys. Polon.* **B 12** (1981) 347; *Act. Phys. Austr.* Suppl. XXIV (1982) 203.
I.Y. Bigi, Yu.L. Dokshitzer, V.A. Khoze, J.H. Kühn, and P.M. Zerwas, *Phys. Lett.* **B 181** (1986) 157.

[3] V.S. Fadin and V.A. Khoze, *Z. Phys.* **C 46** (1987) 417 [*JETP Lett.* **46** (1987) 525]; *Yad. Fiz.* **48** (1988) 487 [*Sov. J. Nucl. Phys.* **48** (1988) 309].

[4] M.J. Strassler and M.E. Peskin, *Phys. Rev.* **D 43** (1991) 1500.

[5] Y. Sumino, K. Fujii, K. Hagiwara, H. Murayama, and C.K. Ng, *Phys. Rev.* **D 47** (1993) 56.

[6] M. Jeżabek, J.H. Kühn and T. Teubner, *Z. Phys.* **C 56** (1992) 653.

[7] M. Jeżabek and T. Teubner, *Z. Phys.* **C 59** (1993) 669.

[8] A. Juste, M. Martinez and D. Schulte, in e^+e^- *Linear Colliders: Physics and Detector Studies*, DESY Orange Report 97-123E;
P. Comas, R. Miquel, M. Martinez, and S. Orteu, in e^+e^- *at TeV Energies: The Physics Potential*, DESY Orange Report 96-123D;
P. Igo-Kemenes, M. Martinez, R. Miquel, and S. Orteu, in e^+e^- *at 500 GeV: The Physics Potential*, DESY Orange Report 93-123C.

[9] H. Murayama, Y. Sumino, *Phys. Rev.* **D 47** (1993) 82.

[10] R. Harlander, M. Jeżabek, J.H. Kühn, and T. Teubner, *Phys. Lett.* **B 346** (1995) 137.

[11] R. Harlander, M. Jeżabek, J.H. Kühn, and M. Peter, *Z. Phys.* **C 73** (1997) 477.

[12] M. Peter and Y. Sumino, *Phys. Rev.* **D 57** (1998) 6912.

[13] A.H. Hoang and T. Teubner, *Phys. Rev.* **D 58** (1998) 114023.

[14] K. Melnikov and A. Yelkhovskii, *Nucl. Phys.* **B 528** (1998) 59.

[15] O. Yakovlev, University of Würzburg Preprint WUE-ITP-98-036 and `hep-ph/9808463`.

[16] R. Brinkmann et al. (Eds.), *Conceptual Design of a 500 GeV e^+e^- Linear Collider with Integrated X-ray Laser Facility*, DESY 1997-048 and ECFA 1997-182.

[17] V.S. Fadin, V.A. Khoze and A.D. Martin, *Phys. Lett.* **B 320** (1994) 141; *Phys. Rev.* **D 49** (1994) 2247.

[18] K. Melnikov and O. Yakovlev, *Phys. Lett.* **B 324** (1994) 217; *Nucl. Phys.* **B 471** (1996) 90.

[19] V.S. Fadin, V.A. Khoze and M.I. Kotskii, *Z. Phys.* **C 64** (1994) 45.

[20] V.S. Fadin and V.A. Khoze, *Sov. J. Nucl. Phys.* **53** (1991) 692.

[21] I.I. Bigi, V.S. Fadin, V.A. Khoze, *Nucl. Phys.* **B 377** (1992) 461.

[22] R. Barbieri, R. Kögerler, Z. Kunszt, and R. Gatto, *Nucl. Phys.* **B 105** (1976) 125.

[23] J.H. Kühn and P.M. Zerwas, *Phys. Rep.* **167** (1988) 321.

[24] M. Peter, *Nucl. Phys.* **B 501** (1997) 471; *Phys. Rev. Lett.* **78** (1997) 602.
Y. Schröder, DESY Orange Preprint 98-191 and `hep-ph/9812205`, *Phys. Lett.* **B** (in press).

[25] M. Jeżabek, J.H. Kühn, M. Peter, Y. Sumino, and T. Teubner, *Phys. Rev.* **D 58** (1998) 14006.

[26] R. Harlander, Diploma thesis (in German), University of Karlsruhe, 1995, unpublished.

[27] B. Grazadkowski, P. Krawczyk, J.H. Kühn, and R.G. Stuart, *Nucl. Phys.* **B 281** (1987) 18.

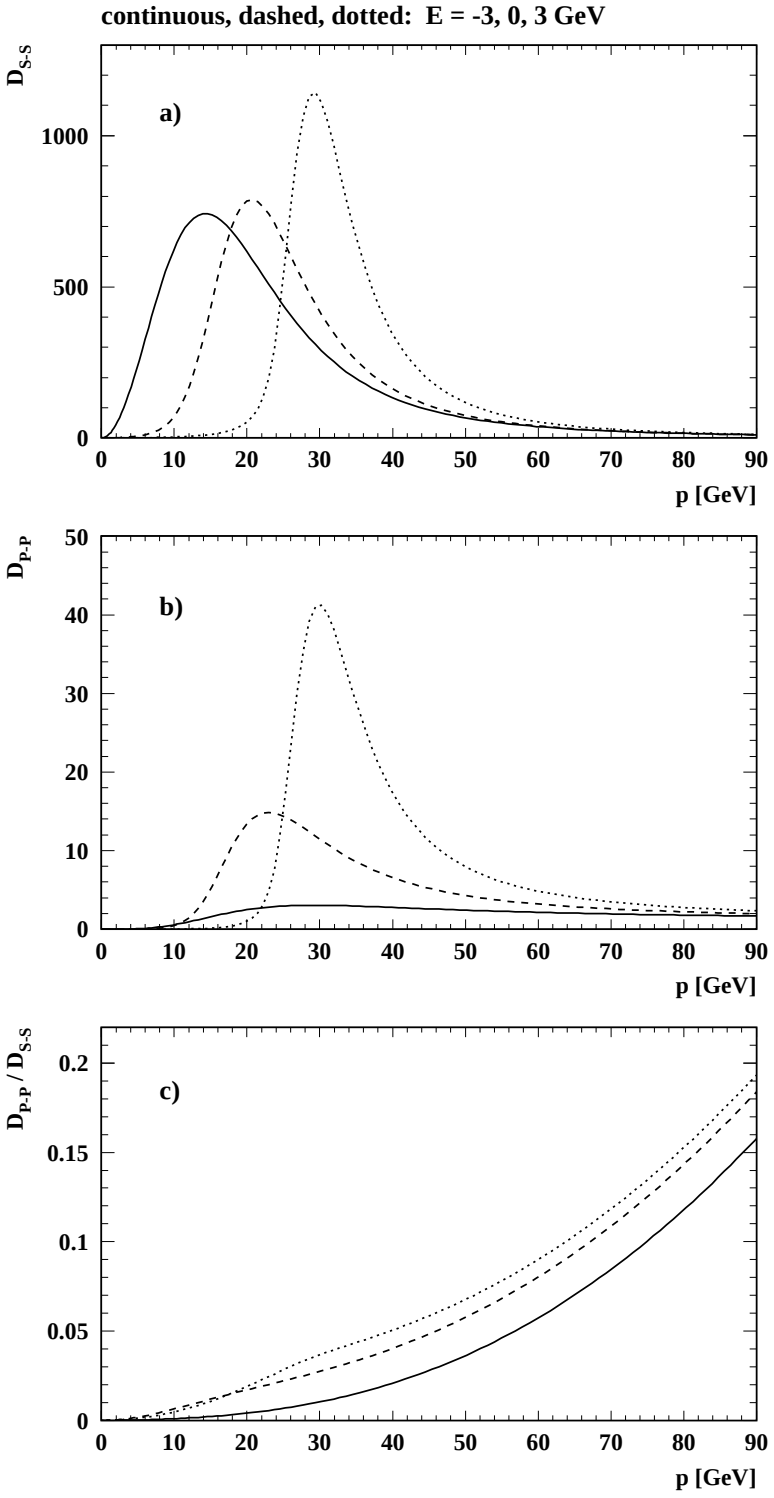

Figure 1: Results for the basic elements in Eq. (1): a) $\mathcal{D}_{S-S}(p,E)$, b) $\mathcal{D}_{P-P}(p,E)$ and c) the ratio $\mathcal{D}_{P-P}/\mathcal{D}_{S-S}$ for the three energies $E=-3$ GeV (continuous curves), $E=0$ (dashed lines) and $E=3$ GeV (dotted) as a function of the top quark momentum p.

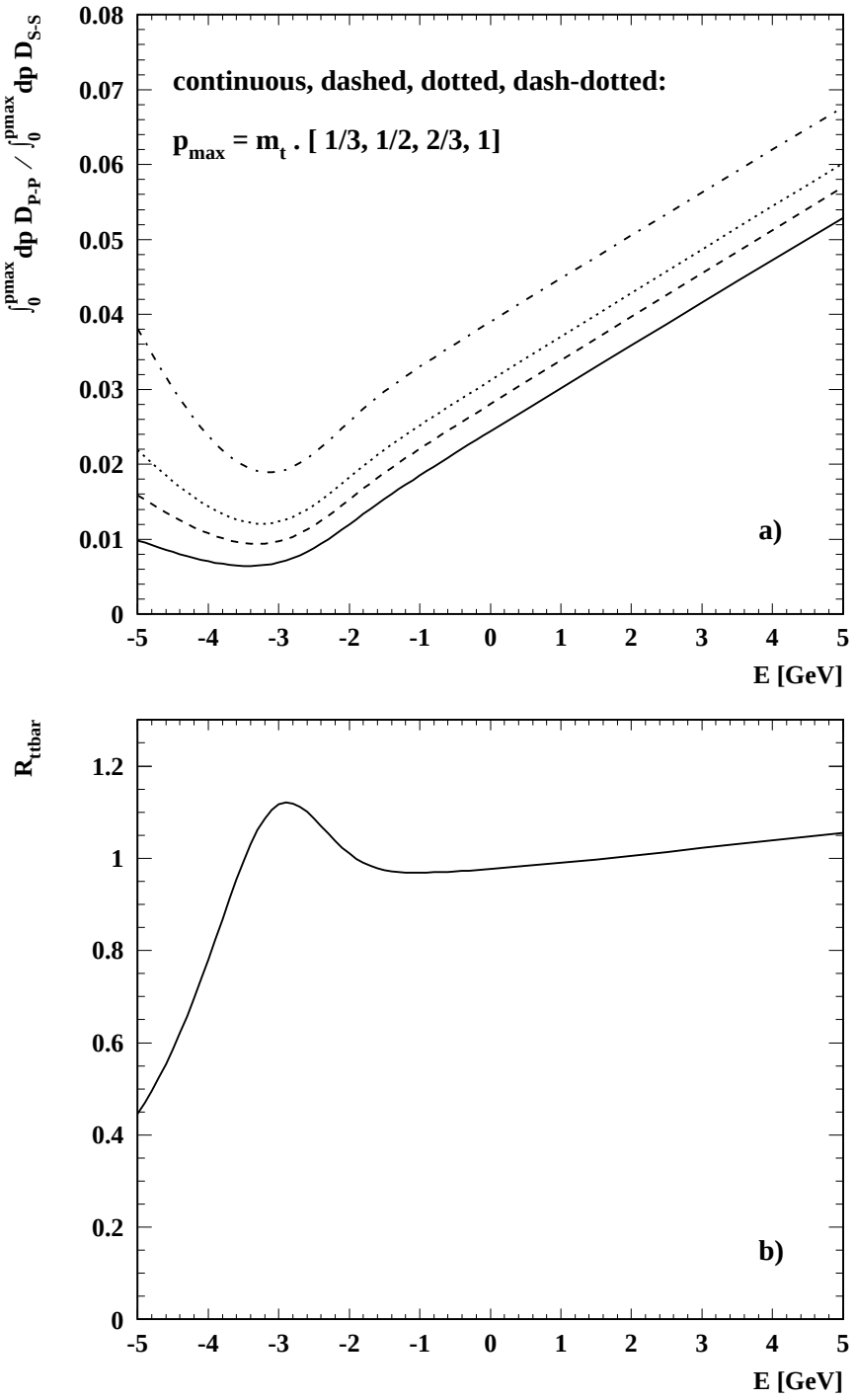

Figure 2:
a) Ratio of the integrated distributions: $\int_0^{p_{\max}} \mathrm{d}p\, \mathcal{D}_{P-P}(p,E)$ / $\int_0^{p_{\max}} \mathrm{d}p\, \mathcal{D}_{S-S}(p,E)$ as a function of the energy $E = \sqrt{s} - 2m_t$ for four different values of the cutoff: continuous, dashed, dotted, and dash-dotted lines correspond to $p_{\max} = m_t \cdot \left[\frac{1}{3},\ \frac{1}{2},\ \frac{2}{3},\ 1\right]$, respectively. b) The normalized total cross section $R_{t\bar{t}}$ as defined in Eq. (9) as a function of E.

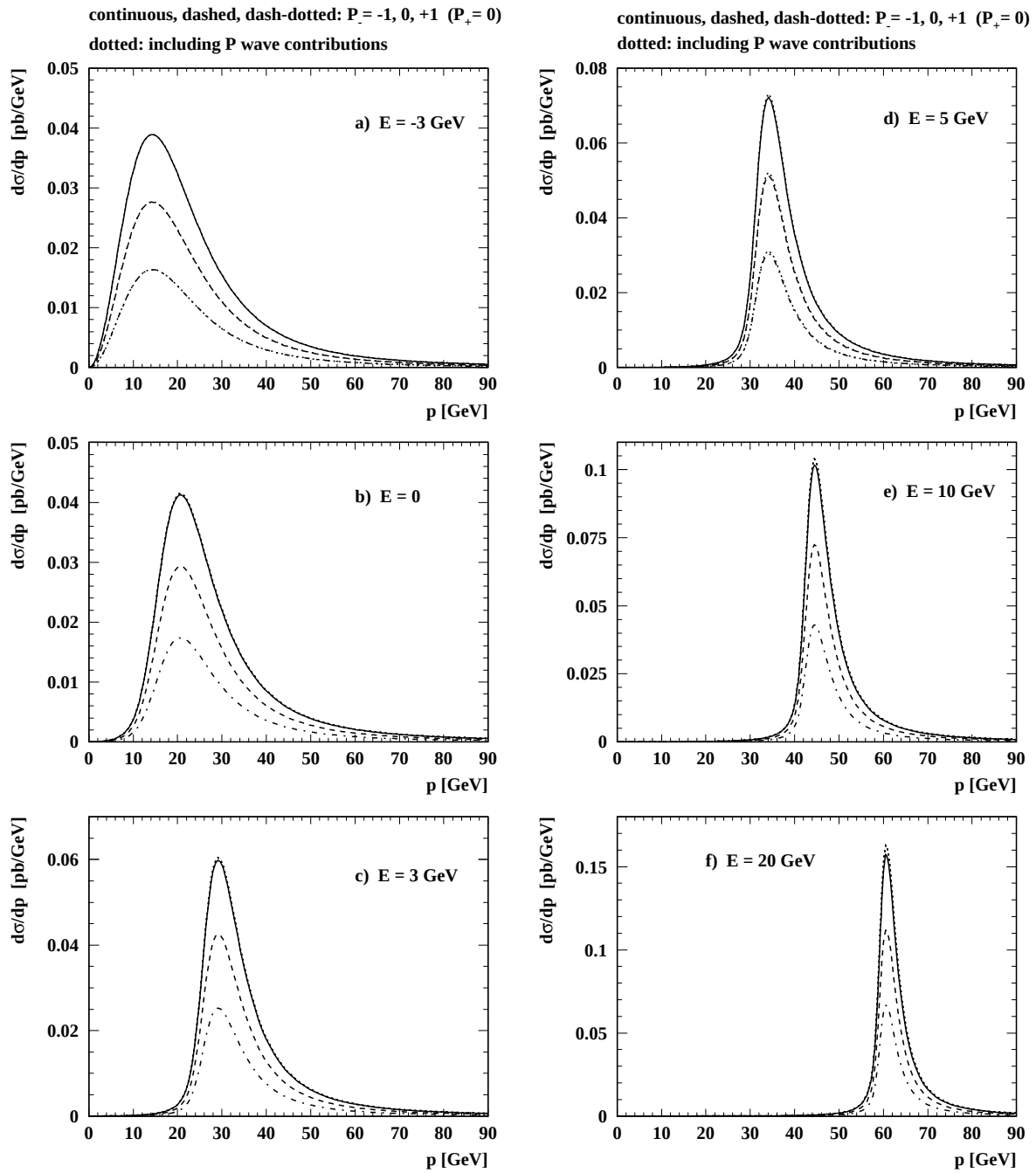

Figure 3: Differential cross section $\mathrm{d}\sigma(e^+e^- \to t\bar{t})/\mathrm{d}p$ as defined in Eq. (1) as a function of p for six different energies, $E = -3, 0, 3, 5, 10, 20$ GeV, as indicated in the plots a)... f). The continuous, dashed and dash-dotted lines show the pure S wave result for the three different choices of the e^- polarization $P_- = -1$, 0 and 1, respectively. ($P_+ = 0$.) The dotted lines show the full result including the P wave contributions.

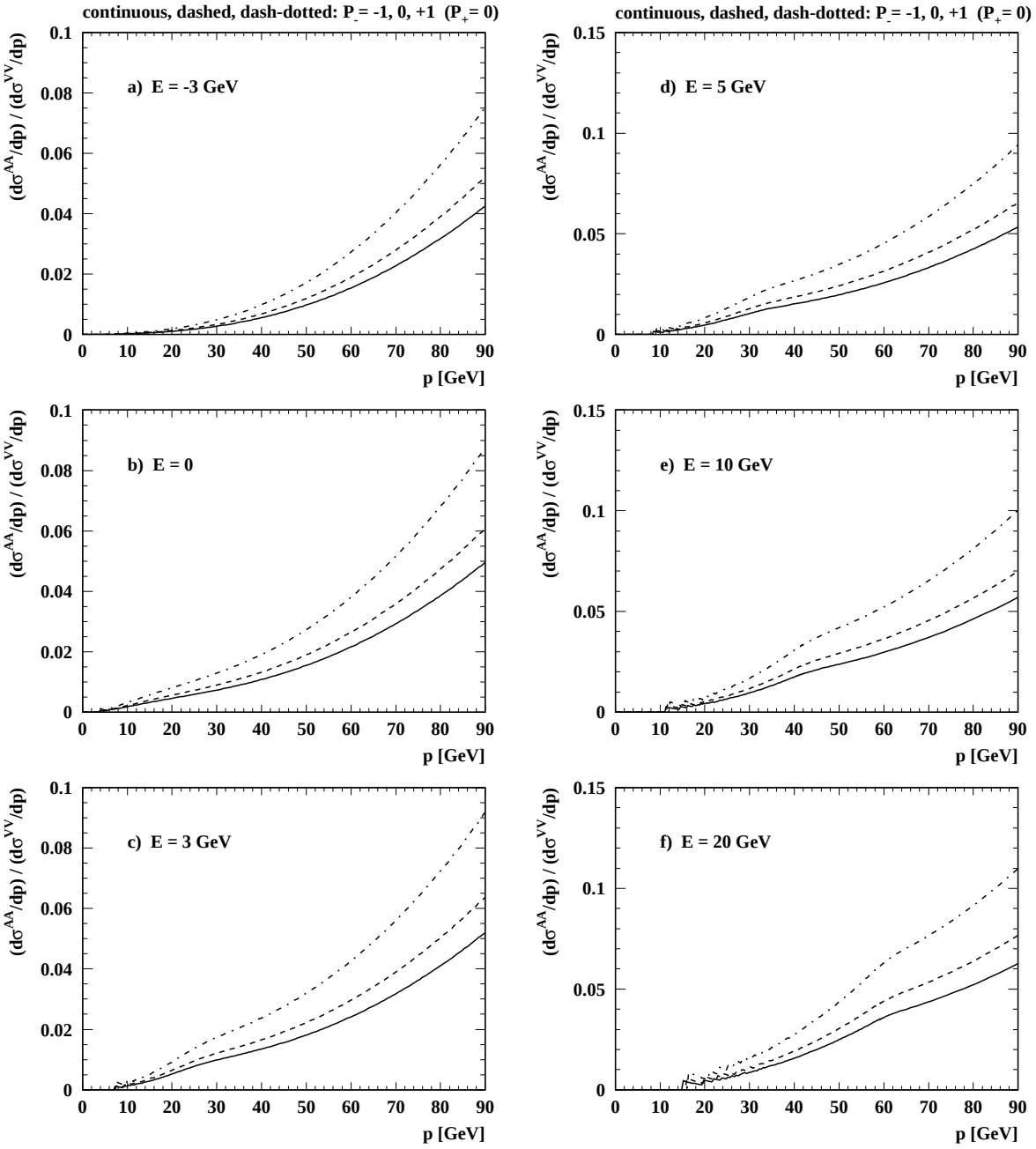

Figure 4: Relative size of the axial contribution $\mathrm{d}\sigma^{\mathrm{AA}}/\mathrm{d}p$ compared to the vector contribution $\mathrm{d}\sigma^{\mathrm{VV}}/\mathrm{d}p$ to the differential cross section as a function of p for six different values of the energy E [plots a)... f)]. The continuous, dashed and dash-dotted lines correspond to $P_- = -1$, 0 and 1, respectively. ($P_+ = 0$.)

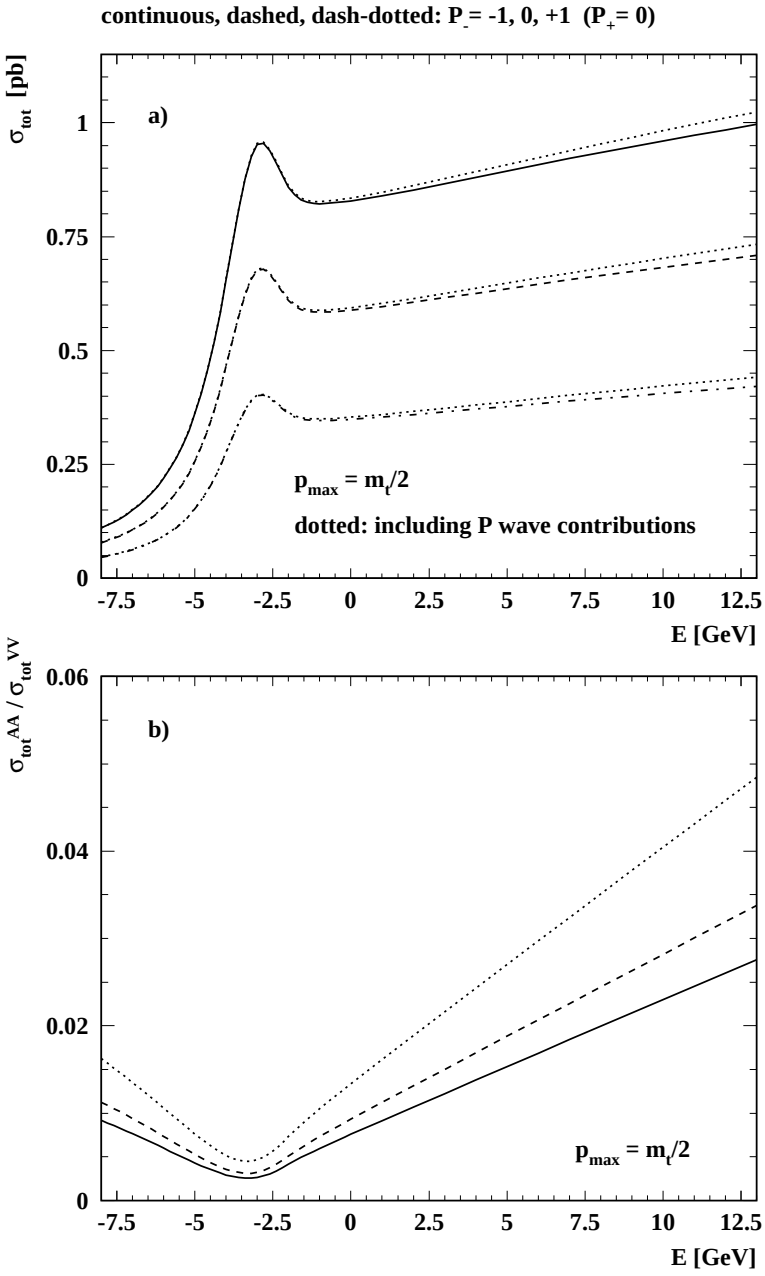

Figure 5: a) The total cross section $\sigma(e^+e^- \to t\bar{t}\,)$ as a function of E for three different choices of the e^- polarization: the continuous, dashed and dash-dotted lines correspond to $P_- = -1$, 0 and 1, respectively, where only S wave production is taken into account. The dotted lines show the corresponding total cross sections including the P wave contributions. b) Ratio of the P to the S wave contribution $\sigma_{\rm tot}^{\rm AA}/\sigma_{\rm tot}^{\rm VV}$ for the three different e^- polarizations.